Population Density Extraction of Kirkuk City Using Landsat Thermal Band and GIS

Kamalaldin F. Hasan[1] [1]Department of Surveying Techniques Engineering, Technical Engineering College of Kirkuk, Northern Technical University, Kirkuk 36001, Iraq.

Iman Ali Shawkat[2] [2]Department of Civil Engineering, College of Engineering, Kirkuk University, Kirkuk 36001, Iraq.

Qayssar Mahmood Ajaj[1*] *Corresponding author: Qayssar Mahmood Ajaj, Department of Surveying Techniques Engineering, Technical Engineering College of Kirkuk, Northern Technical University, Kirkuk 36001, Iraq. E-mail: qayssarrsgis@gmail.com

ABSTRACT

Population and population density estimates become more difficult to make in countries with rapid population growth, shifting immigration patterns, and other forms of unpredictable demographic change. It is, therefore, crucial to conduct a population count rapidly and cheaply; one viable option for doing so is to make use of satellite photos that feature thermal bands. We used a method (Spatial Analyst) and an idea from statistics that deals with clusters of data to determine the arithmetic means of the correlations between land surface temperature and population density. This study makes use of 2019 Landsat satellite pictures and population density information collected from the Kirkuk Governorate. The calculated conversion factors were the result of applying spatial analysis and statistical analysis to the 13 regions we provided. 2300.00, 898.65, 830.81, 668.65, 585.49, 559.66, 509.28, 452.69, 412.71, and 241.57 for temperatures of 30.5, 31.5, 32.5, 33.5, 34.5, 35.5, 36.5, 37.5, 38.5, and 39.5 Celsius respectively.

Keywords: *Population density, Landsat imagery, thermal bands, GIS*

1. Introduction

The easiest way to generate a grid density map is to gather person data with dwelling coordinates, and to count the number of people in each grid cell (bottom-up app) (Gallego et al., 2020). But this approach can be costly and time-consuming. Because of the increase in slums and abuse cases in the Kirkuk region, as with the rest of Iraq, many residential units are not officially registered in state properties, complicating the problem further. The ability to generate a country's reliable population map easily and cost-effectively has many advantages. In addition, during natural disasters, such as earthquakes and flooding, a reliable population map will help coordinate relief operations more quickly and more efficiently (Hu et al., 2019). Cities urgently need to provide accurate and precise population distribution information in order to enhance urban governance (Zhao & Yang, 2020).

To investigate how individuals engage with their immediate physical and social surroundings, we need geospatial population density data at the building level. At this size, high-resolution aerial pictures are seen as a potential tool for mapping urban characteristics because of the way they capture

spatial dynamics (Ural et al., 2011). Residential and commercial zones are clearly delineated on city maps. Detailed instructions are provided for extracting building types from photographs and other GIS data layers (Ural et al., 2011). In a dynamic way, urbanization transforms rural lifestyles into urban ones. It's the process by which a region's physical boundaries and social and economic structures evolve, as well as the broader shift from undeveloped to developed land uses (Makhamreha & Almanasyeha, 2011). Nonetheless, cities are dynamic ecosystems that change over time, and satellite pictures can be used to monitor changes to spatial characteristics of landscape patterns (Dietzel et al., 2005). Strong population growth in urban areas has culminated in large-scale vegetation and climate change. More land must be developed as a city grows to accommodate public infrastructure (such as roadways, water services, and utilities), housing, and commercial and industrial applications (Satterthwaite et al., 2010). This has been shown to be the case (Satterthwaite et al., 2010). Researchers have known for over a decade that the technical challenges of integrating human geography and data collected from distant sensing sources is a deterrent to widespread adoption of satellite data. (Rindfuss & Stern, 1998).

When compared to the expense of collecting nationally representative population census or home survey data, the cost of obtaining satellite photographs across expansive regions is comparatively modest (Guoping et al., 2001). Standard demographic data sets would not follow these requirements, as censuses seldom, generally for decades, provide local population statistics (Engstrom et al., 2019).

Traditionally, census was the main source of knowledge on population density and demographics (Liu et al., 2013). Population distribution was analyzed using a wide range of satellite imagery, including Landsat MSS (Iisaka & Hegedus, 1982), TM and ETM (Li & Weng, 2005), SPOT (Liu et al., 2013), and DMSP night-time imagery (Satterthwaite et al., 2010). Research on the need of spatial resolution for applications with a limited service area varies in quality but is widely accepted of between 0.5 and 5.0 m. (Makhamreha & Almanasyeha, 2011). Using Landsat thermal bands and a geographic information system, our research hopes to deduce both population density and a working factor.

Methods and materials

The methodology is summarized by converting the thermal band 10 of the Landsat satellite image 2019 to the Land Surface Temperature (LST). To find factors for each temperature degree, which can be applied to any other sectors to determine the population density, the extracted temperature is treated with the established population density of those sectors. When density values are measured, they are compared to the density of the sector in consideration to verify for validity. Figure 1 illustrates the overall methodologies of this research.

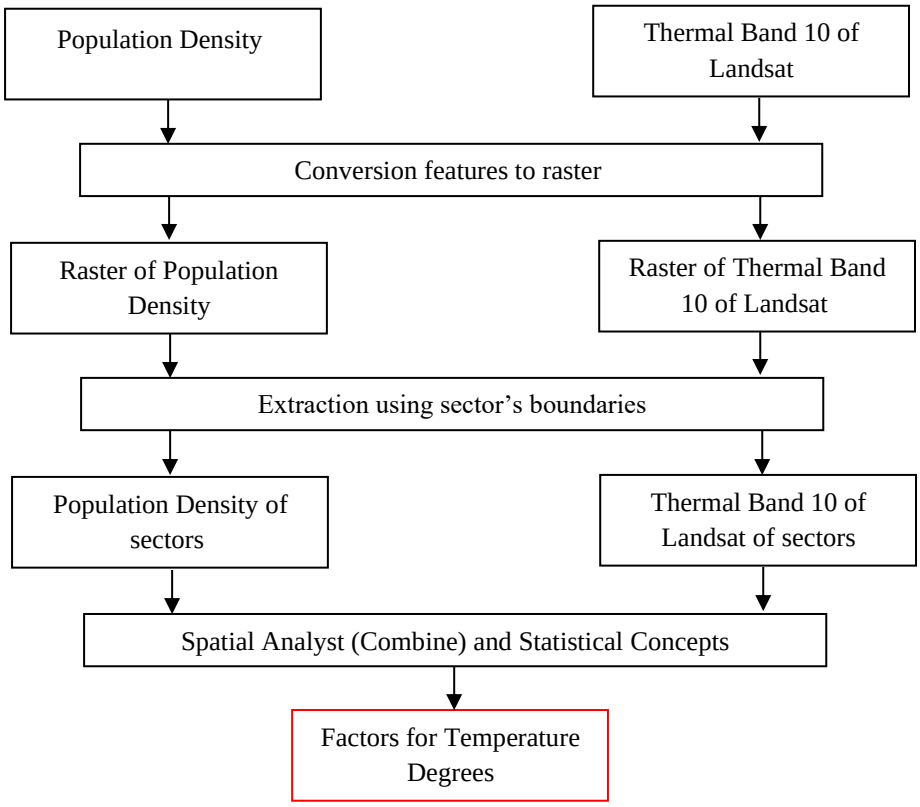

Figure 1: Flowchart of the methodology

Study area

The study area is in Kirkuk, 286 km north of Iraq's capital Baghdad. It sits between latitudes (35˚23' and 35˚32'), and between longitudes (44˚26' and 44˚18'), with a mean elevation of 350 m. Its approximate area is 9,679 km^2 and constitutes 2.2 percent of Iraq's total territory. It is bordered by the Zakros Mountains from the north, the small Zab River from the west, the Hamrin Mountains from the south-west and the Diyala River from the south-west. The Al-Khassa River passes through the middle of Kirkuk City and divides the city into two parts .The small Zab River (one of the most significant tributaries of the Tigris River) passes approximately 45 km from the centre of the city. Kirkuk has seven industries. In 2010, the population of Kirkuk City was reported to be 1,475,711, compared to 753,171 in 1997, and with an increase of 3.4% of the total population in Iraq (Omar et al., 2020). These areas were found to have a distinct difference in population densities among them when humans started settling in this area after development; the area's settlement density was higher than before. Figure 2 states the area of study which is Kirkuk City.

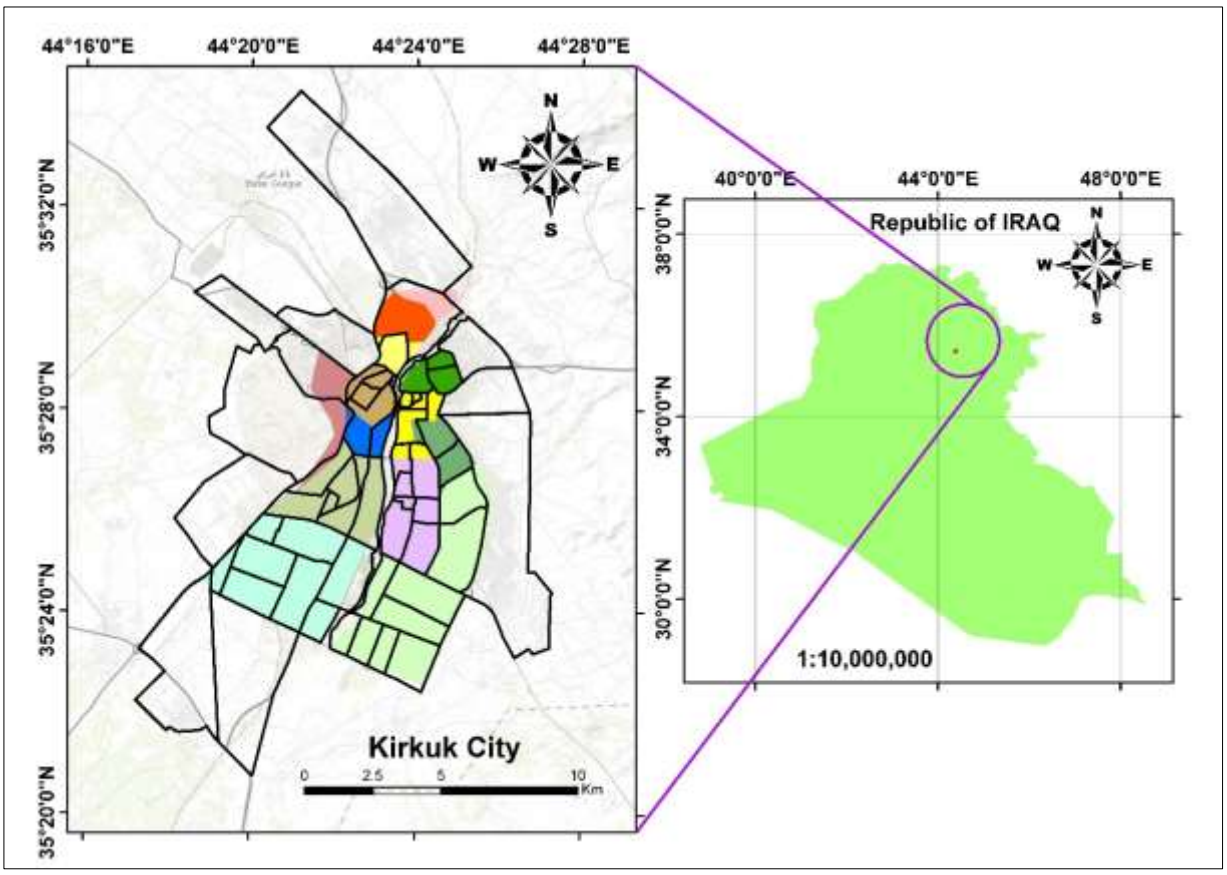

Figure 2: Study area (Kirkuk City)

Data used

A high-resolution aerial photograph, sector boundaries, and the population density of Kirkuk City were obtained from the Kirkuk Governorate. Some population densities of the sectors were checked using population data from the main Kirkuk supply branch. Satellite image Landsat-8 OLI for 2019 within WRS-2 (path 169 row 35) data sets were downloaded. The 30-meter spatial resolution, 16-day temporal resolution, and 12-bit radiometric resolution of the Landsat-8 OLI sensor are comparable to those of the Landsat-7 ETM+, with the exception of the deep-blue coastal/aerosol and short-wave cirrus bands (Ajaj et al., 2017). The thermal bands that are included in Landsat-8 OLI were used to extract the emitted temperature.

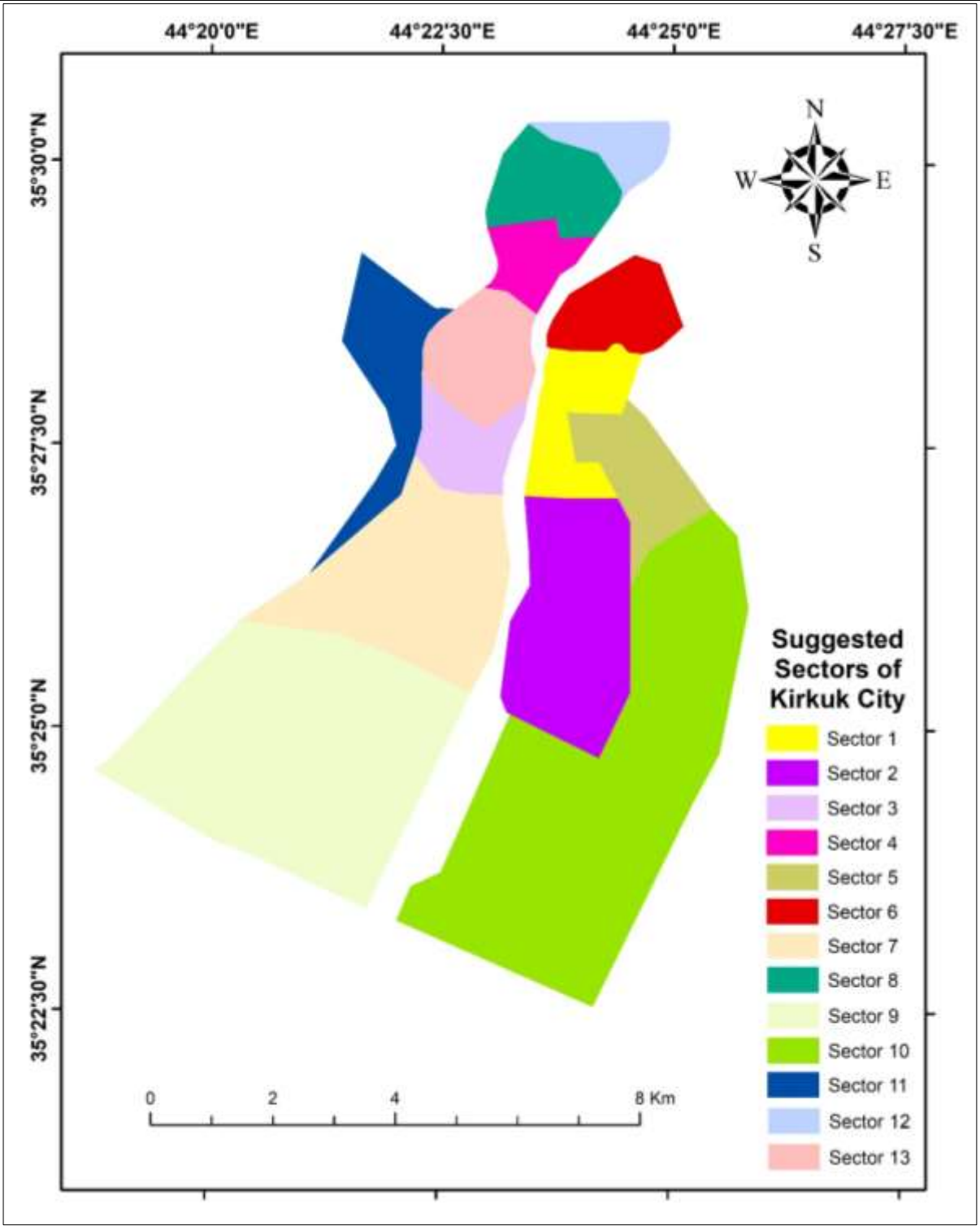

Figure 3: Selected sectors of Kirkuk City

Extract the temperature from thermal bands

Table 1 presents the required metadata for a satellite image in order to estimate temperature from thermal, red, and infrared bands of Landsat. The conversion process can be achieved via several steps, which are (F. Wang et al., 2015):

1. Converting digital number (DN) values of band 9.9 (thermal infrared 10.7 - 11.20 μm wavelength, with spatial resolution equal to 100 m) Regarding

spectrum radiation measured by an at-sensor device, we get the following formula:

$$L_\lambda = \frac{(L_{max} - L_{min})\ Q_{cal}}{(Q_{calmax} - Q_{calmin})} + L_{min} - O_i \quad (1)$$

Where,

L_{max} is the maximum radiance (W.m $^{-2}$.sr^{-1}.μm^{-1})

L_{min} is the minimum radiance (W.m $^{-2}$.sr^{-1}.μm^{-1})

Q_{cal} is the digital number value of pixels

Q_{calmax} is the highest possible value for a pixel's digital digit

Q_{calmin} represents the lowest possible pixel value in a digital representation

O_i band 9.9's appropriate adjustment value

Table 1: Required variables in metadata of Landsat satellite image for extracting the temperature

Items description	The values
Thermal constants (K_1 and K_2), band 10.1	K_1 = 774.8853 K_2 = 1321.0789
Radiance Extremes and Minimums (λ_{max} and λ_{min}), band 10.1	λ_{max} = 22.00180 λ_{min} = 0.10033
Limits and Extremes of Quantised Calibration (Q_{calmax} and Q_{calmin}), Band 10.1	Q_{calmax} = 65535 Q_{calmin} = 65535
Correction value (Oi), Band 10.1	O_i = 0.29

2. Using the thermal constants of TIR band 9.9 (K1 and K2) found in the satellite image's metadata, we can convert the TIRS band to brightness temperature (BT), as shown below: $BT = \frac{K_1}{\ln\left[\left(\frac{K_2}{L_\lambda}\right)+1\right]} - 273.15$ (2)
   It is necessary to revise the results in Celsius by adding an absolute zero, which is approximately -273.15. The atmospheric impact is not taken into account in retrieving the LST because the study area is relatively dry.
3. Computing the Normalised Difference Vegetation Index (NDVI) to understand the different forms of land cover in the study area. The red band (0.65 - 0.68 μm) and the near infrared band (0.86 - 0.89 μm) of the photos are utilized in the calculation to calculate the NDVI:

   $$NDVI = \frac{(NIR - Red)}{(NIR + Red)} \quad (3)$$

4. Calculating proportional vegetation (P_v) to provide the estimation of the area within each type of land cover. The following equation can be used to determine P_v:

   $$P_v = \left(\frac{NDVI - NDVI_s}{NDVI_v - NDVI_s}\right)^2 \quad (4)$$

   Under global circumstances, it has been proposed that NDVIv = 0.6 and NDVIs = 0.3 be used. In rare instances, the result for vegetated surfaces (NDVIv = 0.6) might be excessively low, and $NDVI_v$ may exceed 0.8 or 0.9 for higher resolution data over agricultural areas (Sun et al., 2010).

5. Calculation of land surface emissivity (ε_λ) (LSE) is necessary to estimate land surface temperature. Specifically, the high emissivity of the land itself acts as a proportionality factor in scaling the black body radiance (Plank's law) to compute emitted radiance, allowing for the transmission of thermal energy from

the surface into the atmosphere. Furthermore, the LSE is largely dependent on the external roughness and condition of vegetation cover, etc. The equation for ε_λ is:

$$\varepsilon_\lambda = \varepsilon_{V\lambda} P_V + \varepsilon_{S\lambda}(1 - P_V) + C_\lambda \quad (5)$$

Where,

ε_v is the vegetation emissivity

ε_s is the soil emissivity

Roughness of the surface, denoted by the constant C = 0.006

Compared to the Earth's surface, aquatic bodies have a very consistent emissivity. Since the emissivity of a terrestrial surface varies with wavelength, the NDVI threshold technique (NTM) may be used to provide estimates of emissivity in the range of 10.2 to 12.3 m.

$$\varepsilon_\lambda = \begin{cases} \varepsilon_{S\lambda,} & NDVI < NDVI_S \\ \varepsilon_{S\lambda} P_V + \varepsilon_{S\lambda}(1 - P_V) + C_\lambda, & NDVI_S \leq NDVI \leq NDVI_S \\ \varepsilon_{S\lambda} + C_\lambda, & NDVI > NDVI_V \end{cases} \quad (6)$$

Table 2: NDVI and emissivity for land cover classes (Jeevalakshmi et al., 2017)

Land cover class	NDVI	Emissivity
Water	Less than 0	0.991
Soil	0 – 0.2	0.996
Mixture of soil and	0.2 – 0.5	
Vegetation	More than 0.5	0.973

6. Finally, calculation of land surface temperature using the following equation:

$$T_s = \frac{BT}{\{1+[(\lambda BT/\rho)\ln \varepsilon_\lambda]\}} \quad (7)$$

Where,

T_s is the LST in Celsius (^oC)

BT is at-sensor BT (^oC)

λ is the average wavelength of band 10

ρ is $h.\frac{c}{\sigma}$

σ is the Boltzmann constant (1.38 x 10^{-23} J/K), h is Plank's constant (6.626 x 10^{-34}) and c is the speed of light (3 x 10^8 m/s).

The presented equations were implemented in the GIS through spatial analysis and the temperature map is shown in figure 4.

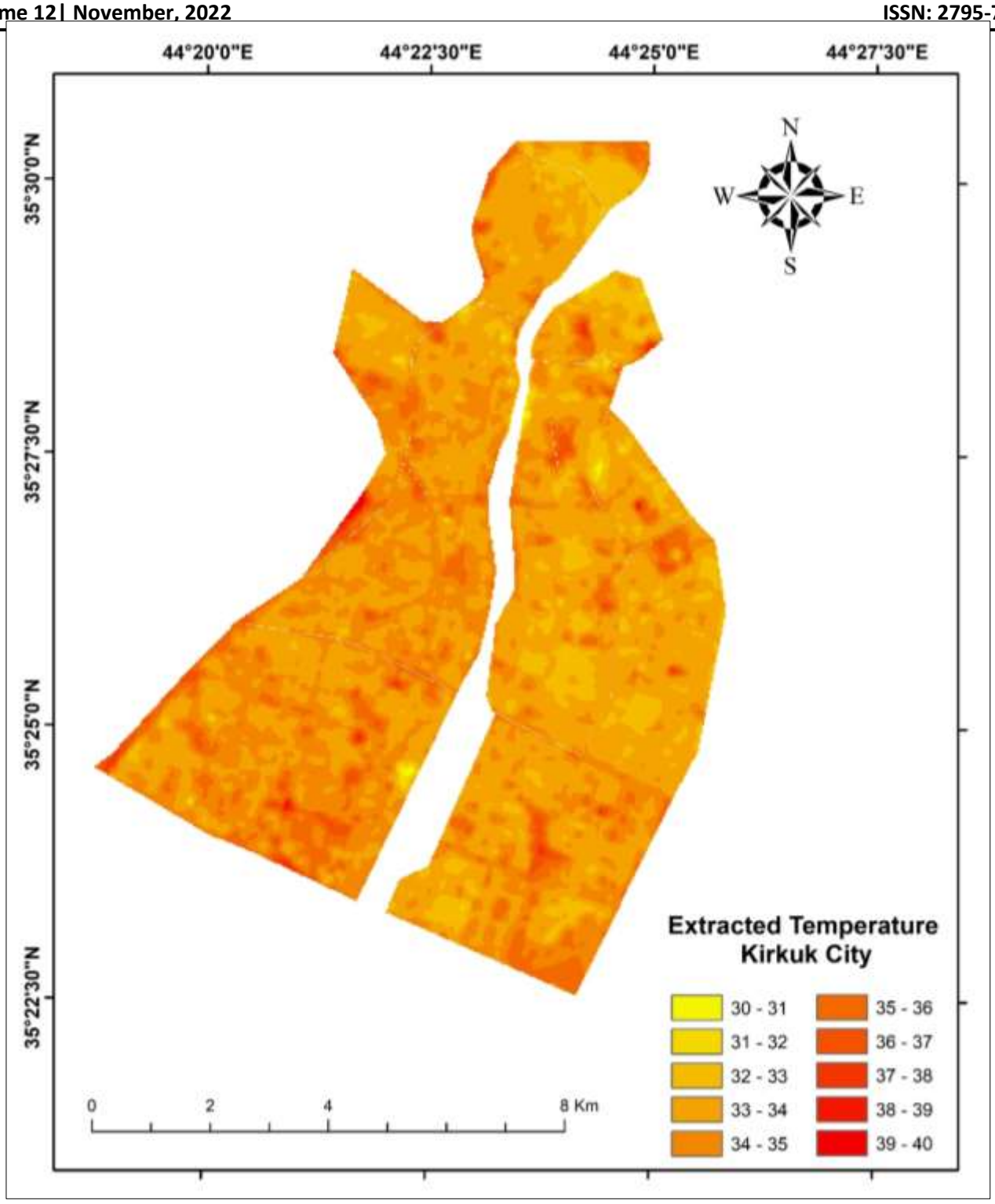

Figure 4: The Temperature in Celsius for Kirkuk City

Population density

Population in sociology refers to other people's set area for a period of time. In compliance with the *Succinct Report* in 2014, the population of the planet heights of 7.3 were attained. billion, and its status may be described as diversified yet unremarkable (United Nations, 2014). Census data at country level are usually acquired once every 10 years. However, quick shifts in local population may be brought about by things like war, migration, urbanization, and natural catastrophes (Engstrom et al., 2019). Applications including environmental change, urbanization, regional planning, public health, and crisis management might all benefit from better understanding

population distributions in space. To evaluate populations with large numbers of people and variance in their distribution, new data processing and specialisation models are needed (L. Wang et al., 2018). In our study, vector files of the population density involve the population number and other parameters. The population densities of all sectors of Kirkuk City were calculated by computing the area of each sector with the number of people to satisfy the obtained data that clear in figure 5.

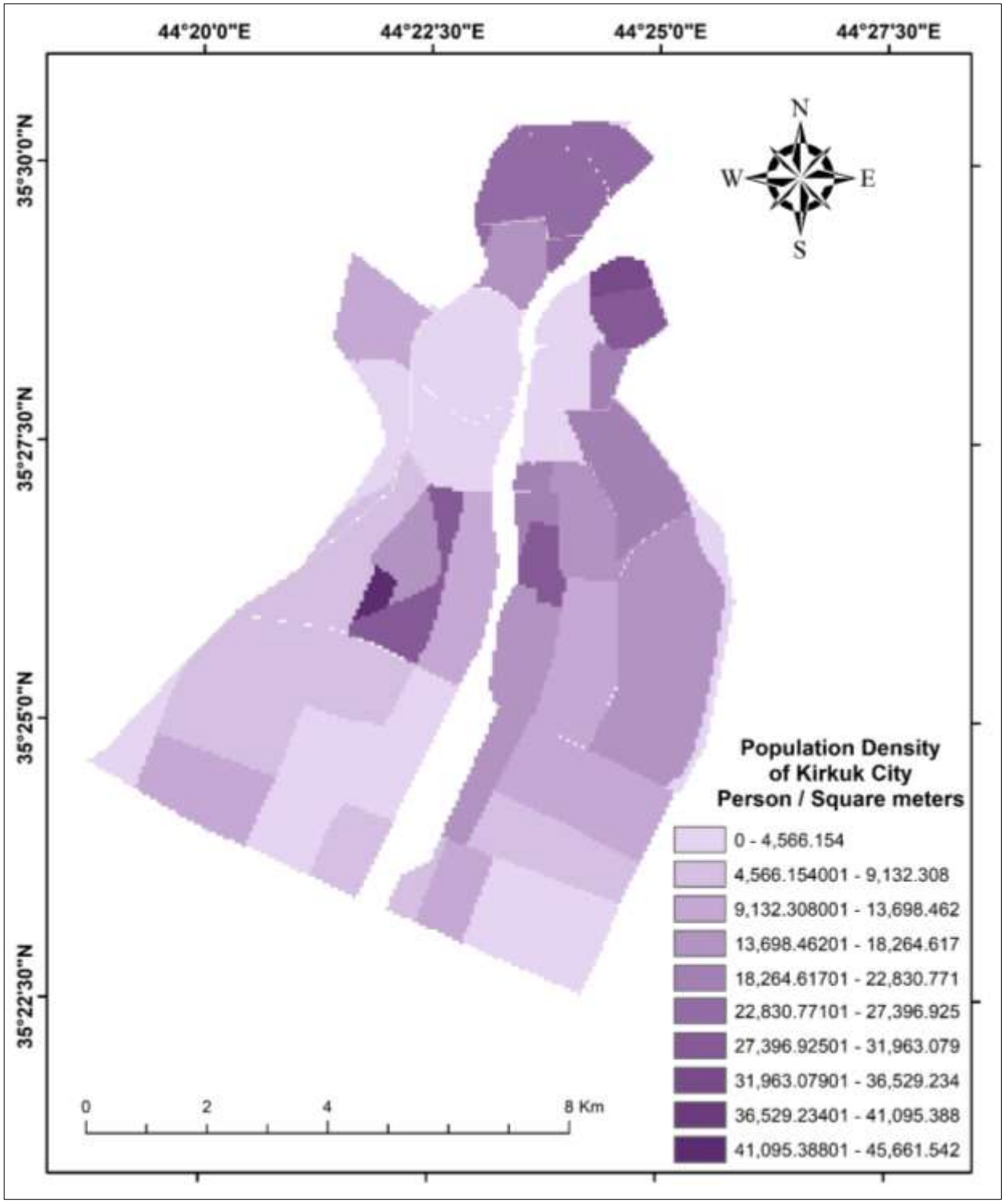

Figure 5: The population density for Kirkuk City

Spatial analysis

Spatial analyses are frequently referred to as the collection of geographical evaluation procedures where analysis findings depend on the spatial organisation of the events (Fotheringham, S., & Rogerson, 2013). The Raster Calculator is a versatile tool that may be used for a wide variety of purposes, including but not limited to doing mathematical calculations using operators and functions, creating selection queries, and entering map algebra syntax (Ajaj et al., 2017). The input is represented by raster datasets or raster layers, coverages, shape files, tables, constants, and numbers. The raster layers of population density and temperature are used to extract the output layers of income factors (Ballas, D., Clarke, G., Franklin, R. S., & Newing, 2017). In this study we used a combined tool for temperature (Celsius) and population density (persons / square meter), with raster layers (13 layers) to obtain most much classes between them for each temperature.

Statistical computations

A frequency distribution aids in the detection of patterns in data by putting some order on the inevitability of fluctuation among observations (Witte & Witte, 2017). The weighted arithmetic mean can be calculated mathematically using equation 8 as follows (Schlossmacher, 1973):

$$W = \frac{\sum_{i=1}^{n} w_i \, X_i}{\sum_{i=1}^{n} w_i} \quad (8)$$

Where,

W is the average weighted mean

n is the number of terms or items in a series to be averaged

w_i are the weights pertaining to x values

X_i are the data values to be averaged

X_i = data values to be averaged.

2. Results

The outcomes of this research represent the corresponding classes of emitted temperature and population density, as discussed in the spatial analysis section of the methodology. Figure 6 illustrates the combined values of temperature and population density over Kirkuk City. The values have 10 classes, starting from (1 - 9) and ending with class (77 - 86). Table 3 depicts the temperatures emitted and the corresponding population densities. In addition, the conversion coefficients for 10 temperatures are included in this table, which may be used to estimate population density in a specific area when Landsat thermal bands are present. There is less population density where the land features emit a higher temperature signal. This explains why, in densely populated areas, radiated temperature decreases because the structures and masses in the area absorb the majority of the temperature.

Table 3: Conversion factors derived from emitted temperatures and corresponding population densities of Kirkuk City.

Emitted Temperatures	Population Density	Conversion Factor
30.5	70149.978	2300
31.5	28307.582	898.65
32.5	27001.253	830.81
33.5	22399.93	668.65
34.5	20199.301	585.49
35.5	19867.953	559.66
36.5	18588.764	509.28
37.5	16975.749	452.69
38.5	15889.223	412.71
39.5	9542.09	241.57

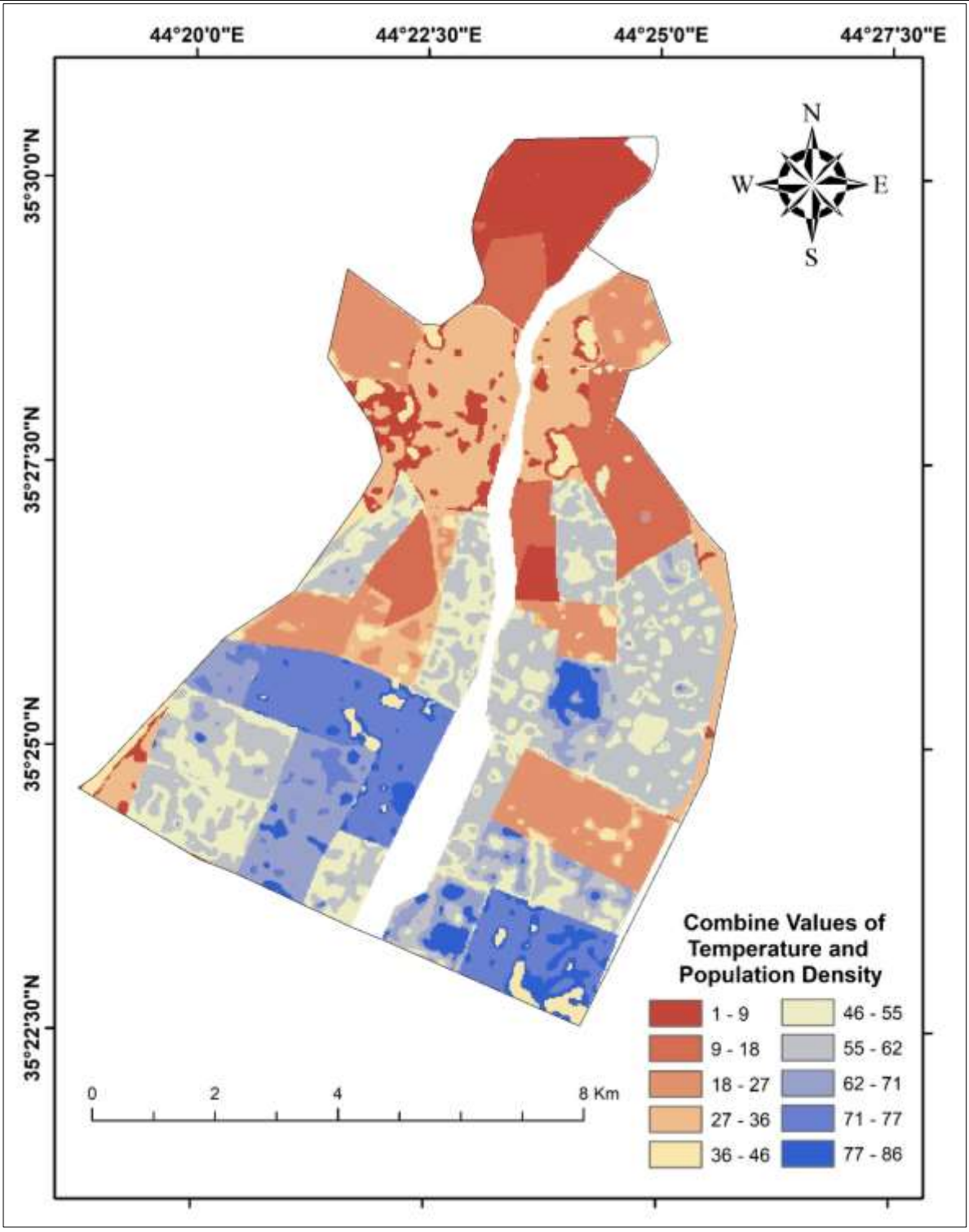

Figure 6: Combine process of temperature degrees and population density over Kirkuk City

3. Conclusion

A fast and inexpensive census process is of great importance, as through this census, it enables the Government to manage services and distribute resources appropriately. This work aims to compute the population density, with the aid of thermal bands in satellite images and a GIS based on statistics. Population density and thermal band 10 of Landsat 2010 for Kirkuk City and its parameters were used as data in this research. The results of this study were temperatures of 30.5, 31.5, 32.5, 33.5, 34.5, 35.5, 36.5, 37.5, 38.5, and 39.5 Celsius, and computed

conversion coefficients were 2300.00, 898.65, 830.81, 668.65, 585.49, 559.66, 509.28, 452.69, 412.71, and 241.57. Where the terrain features emit a higher temperature signal, there is less population density. This indicates why radiated temperature drops in highly populated regions, since the buildings and features in that area play a significant role in absorbing the temperature. Future studies should apply these conversion coefficients between emitted temperature and population densities, in order to confirm validity and extend to further use.

References

1. Ajaj, Q. M., Pradhan, B., Noori, A. M., & Jebur, M. N. (2017). Spatial Monitoring of Desertification Extent in Western Iraq using Landsat Images and GIS. *Land Degradation and Development*, *28*(8). https://doi.org/10.1002/ldr.2775
2. Ballas, D., Clarke, G., Franklin, R. S., & Newing, A. (2017). *GIS and the Social Sciences: Theory and Applications*.
3. Dietzel, C., Herold, M., Hemphill, J. J., & Clarke, K. C. (2005). Spatio-temporal dynamics in California's Central Valley: Empirical links to urban theory. *International Journal of Geographical Information Science*, *19*(2), 175–195. https://doi.org/10.1080/13658810410001713407
4. Engstrom, R., Newhouse, D., & Soundararajan, V. (2019). Estimating Small Area Population Density Using Survey Data and Satellite Imagery: An Application to Sri Lanka. *Estimating Small Area Population Density Using Survey Data and Satellite Imagery: An Application to Sri Lanka*, *March*. https://doi.org/10.1596/1813-9450-8776
5. Fotheringham, S., & Rogerson, P. (Eds. . (2013). *Spatial analysis and GIS*.
6. Gallego, J. A., Perich, M. G., Chowdhury, R. H., Solla, S. A., & Miller, L. E. (2020). Long-term stability of cortical population dynamics underlying consistent behavior. *Nature Neuroscience*, *23*(2), 260–270. https://doi.org/10.1038/s41593-019-0555-4
7. Guoping, Z. G. Z., Jiyuan, L. J. L., & Zenxiang, Z. Z. Z. (2001). Remote sensing investigation of the main sand-supplying areas ofdust storm hitting northern China. *IGARSS 2001. Scanning the Present and Resolving the Future. Proceedings. IEEE 2001 International Geoscience and Remote Sensing Symposium (Cat. No.01CH37217)*, *5*(C), 2097–2099. https://doi.org/10.1109/IGARSS.2001.977915
8. Hu, W., Novosad, P., Burke, M., Patel, J. H., Asher, S., Lobell, D., Robert, Z. A., Tang, Z., & Ermon, S. (2019). Mapping missing population in rural India: A deep learning approach with satellite imagery. *AIES 2019 - Proceedings of the 2019 AAAI/ACM Conference on AI, Ethics, and Society*, 353–359. https://doi.org/10.1145/3306618.3314263
9. Iisaka, J., & Hegedus, E. (1982). Population estimation from Landsat imagery. *Remote Sensing of Environment*, *12*(4), 259–272. https://doi.org/10.1016/0034-4257(82)90039-6
10. Jeevalakshmi, D., Narayana Reddy, S., & Manikiam, B. (2017). Land surface temperature retrieval from LANDSAT data using emissivity estimation. *International Journal of Applied Engineering Research*, *12*(20), 9679–9687.
11. Li, G., & Weng, Q. (2005). Using Landsat ETM+ imagery to measure population density in Indianapolis, Indiana, USA. *Photogrammetric Engineering and Remote Sensing*, *71*(8), 947–958. https://doi.org/10.14358/PERS.71.8.947
12. Liu, X., Clarke, K., & Herold, M. (2013). Population Density and Image Texture. *Photogrammetric Engineering & Remote Sensing*, *72*(2), 187–196. https://doi.org/10.14358/pers.72.2.187
13. Makhamreha, Z., & Almanasyeha, N.

(2011). Analyzing the state and pattern of urban growth and city planning in Amman using satellite images and GIS. *European Journal of Social Sciences*, *24*(2), 252–264.

14. Omar, N. Q., Shawkat, I. A., Ali, S. H., & Abujayyab, S. K. M. (2020). Selection of Suitable Site for Solid Waste Landfill : a case study in Kirkuk City, Iraq. *IOP Conference Series: Materials Science and Engineering*, *737*(1). https://doi.org/10.1088/1757-899X/737/1/012216
15. Rindfuss, R., & Stern, P. (1998). Rindfuss_1998_PandP_Challenges. In *People and Pixels: Linking Remote Sensing and Social Science* (pp. 1–27).
16. Satterthwaite, D., McGranahan, G., & Tacoli, C. (2010). Urbanization and its implications for food and farming. *Philosophical Transactions of the Royal Society B: Biological Sciences*, *365*(1554), 2809–2820. https://doi.org/10.1098/rstb.2010.0136
17. Schlossmacher, E. J. (1973). An iterative technique for absolute deviations curve fitting. *Journal of the American Statistical Association*, *68*(344), 857–859.
18. Sun, Q., Tan, J., & Xu, Y. (2010). An ERDAS image processing method for retrieving LST and describing urban heat evolution: A case study in the Pearl River Delta Region in South China. *Environmental Earth Sciences*, *59*(5), 1047–1055. https://doi.org/10.1007/s12665-009-0096-3
19. United Nations. (2014). Concise report on the world population situation 2014. *Available Online at: Http://Www.Un.Org/En/Development/Desa/Population/Publications/Trends/Concise-Report2014.Shtml,* Accessed date: 1 April 2015.
20. Ural, S., Hussain, E., & Shan, J. (2011). Building population mapping with aerial imagery and GIS data. *International Journal of Applied Earth Observation and Geoinformation*, *13*(6), 841–852. https://doi.org/10.1016/j.jag.2011.06.004
21. Wang, F., Qin, Z., Song, C., Tu, L., Karnieli, A., & Zhao, S. (2015). An improved mono-window algorithm for land surface temperature retrieval from landsat 8 thermal infrared sensor data. *Remote Sensing*, *7*(4), 4268–4289. https://doi.org/10.3390/rs70404268
22. Wang, L., Wang, S., Zhou, Y., Liu, W., Hou, Y., Zhu, J., & Wang, F. (2018). Mapping population density in China between 1990 and 2010 using remote sensing. *Remote Sensing of Environment*, *210*(February), 269–281. https://doi.org/10.1016/j.rse.2018.03.007
23. Witte, R. S., & Witte, J. S. (2017). *Statistics, 11th Edition*.
24. Zhao, G., & Yang, M. (2020). Urban Population Distribution Mapping with Multisource Geospatial Data Based on Zonal Strategy. *ISPRS International Journal of Geo-Information*, *9*(11), 654. https://doi.org/10.3390/ijgi9110654